



PROBING TRAPPIST-1-LIKE SYSTEMS WITH *K2*

BRICE-OLIVIER DEMORY¹, DIDIER QUELOZ¹, YANN ALIBERT², ED GILLEN¹, AND MICHAEL GILLON³

¹Astrophysics Group, Cavendish Laboratory, J.J. Thomson Avenue, Cambridge CB3 0HE, UK; bod21@cam.ac.uk

²Physikalisches Institut & Center for Space and Habitability, Universität Bern, 3012 Bern, Switzerland

³Institut d'Astrophysique et de Géophysique, Université de Liège, Allée du 6 Aout 17, Bat. B5C, B-4000 Liège, Belgium

Received 2016 May 6; revised 2016 June 10; accepted 2016 June 14; published 2016 July 8

ABSTRACT

The search for small planets orbiting late M dwarfs holds the promise of detecting Earth-size planets for which their atmospheres could be characterized within the next decade. The recent discovery of TRAPPIST-1 entertains hope that these systems are common around hosts located at the bottom of the main sequence. In this Letter, we investigate the ability of the repurposed *Kepler* mission (*K2*) to probe planetary systems similar to TRAPPIST-1. We perform a consistent data analysis of 189 spectroscopically confirmed M5.5 to M9 late M dwarfs from Campaigns 1–6 to search for planet candidates and inject transit signals with properties matching TRAPPIST-1b and c. We find no transiting planet candidates across our *K2* sample. Our injection tests show that *K2* is able to recover both TRAPPIST-1 planets for 10% of the sample only, mainly because of the inefficient throughput at red wavelengths resulting in Poisson-limited performance for these targets. Increasing injected planetary radii to match GJ 1214b's size yields a recovery rate of 70%. The strength of *K2* is its ability to probe a large number of cool hosts across the different campaigns, out of which the recovery rate of 10% may turn into bona fide detections of TRAPPIST-1-like systems within the next two years.

Key words: planetary systems – techniques: photometric

1. INTRODUCTION

The recent discovery of TRAPPIST-1 (hereafter T-1; Gillon et al. 2016) from a relatively small target sample ($N \sim 50$) suggests that small planets are frequent around late M dwarfs (hereafter LMDs, M5.5 to M9 spectral type). This discovery indeed confirms that an untapped population of small planets exists around late M hosts, similar to what has been expected from core-accretion models (Payne & Lodato 2007; Alibert et al. 2011). The interest in small planets orbiting LMDs is justified by their enhanced detectability compared to solar analogs and the unprecedented opportunity they offer for atmospheric characterization with near-to-come facilities such as *James Webb Space Telescope* (Seager 2014).

While LMDs are abundant, they are faint in the *Kepler* bandpass (5% throughput at 900 nm; Koch et al. 2010), which limits *Kepler*'s ability to observe them with high precision. Another complicating factor is the *Kepler* data cadence of 30 minutes used for the vast majority of targets, which is similar to typical transit durations of short-orbital-period planets orbiting LMDs. The large collecting area and quasi-continuous monitoring of about 80 days per campaign counterbalance, to some extent, the quenching at longer wavelengths and limited time-sampling of the transits.

Demory et al. (2013) proposed an effort to search for Earth-size planets orbiting LMDs and brown dwarfs with *K2*. In this Letter, we reflect on 1.5 years of *K2* data and the discovery of T-1 to examine how *K2* contributes to the search of planets orbiting LMDs. More specifically, we study the sensitivity of *K2* to planetary systems similar to T-1 and put constraints on the properties of the population of planets orbiting hosts located at the bottom of the main sequence.

2. OBSERVATIONS

K2 has been observing LMDs since Campaign 0. Each corresponding field of view is located close to the ecliptic to

mitigate drifts of the telescope boresight due to differential solar radiation pressure (Howell et al. 2014). *K2* data sets are unprecedented for LMDs because they provide a unique opportunity to search and characterize variability patterns over long timescales compared to the relatively fast rotation period of LMDs (e.g., Reiners & Basri 2010; West et al. 2015).

We base this Letter on a total of 189 M5.5–M9 stars that have been observed in *K2*'s Campaigns 1–6, obtained between 2014 March and 2015 September. The magnitudes in the *Kepler* bandpass range from 14.5 to 23.9. We select only those targets that are confirmed spectroscopically, which allows us to better constrain the host properties for the purpose of transit searches and alleviate contamination from false positives. This selection is done by cross-matching the available *K2* targets with spectroscopically confirmed sources from Cruz & Reid (2002), Cruz et al. (2003, 2007), Lodieu et al. (2007), Reid et al. (2007, 2008), Slesnick et al. (2006, 2008), and West et al. (2008). We use this spectral classification to estimate the radius of each target using evolutionary models (Baraffe et al. 2015). Figure 1 shows the distribution of our target sample as a function of spectral type.

3. DATA ANALYSIS

3.1. Data Reduction

We describe in this section how we perform the data reduction of the *K2* data. Our pipeline uses the *K2* pixel-level files (TPF) as input data. The TPF files are downloaded from the Mikulski Archive for Space Telescopes (MAST⁴). Each TPF file is a data cube that includes all frames for a given target. Each frame contains all pixels included in the mask for a given target. Because of the telescope jitter and repointing, each frame encompasses significant margins along the x and y axes to keep the target in the aperture. As the LMDs observed

⁴ <http://archive.stsci.edu/k2/>

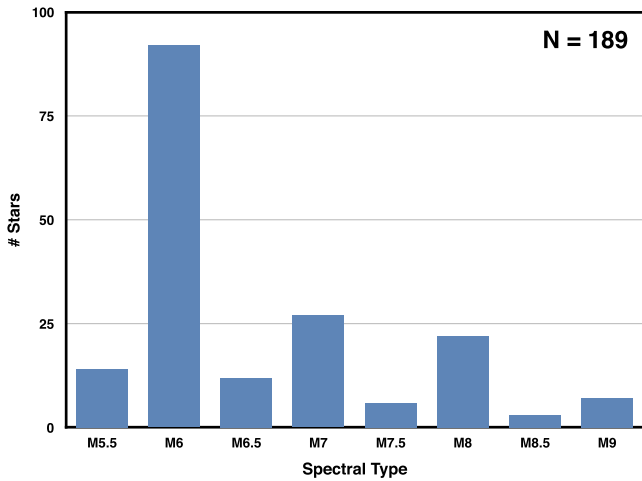


Figure 1. Spectral type distribution of our sample *K2* LMDs. This histogram shows the spectral distribution of targets that are part of our sample during Campaigns 1–6.

within this program are faint and the masks large enough to include other stars (in addition to the ones we are interested in), our code first identifies the location of the star on the frame based on the target coordinates. We then use a PSF centroiding algorithm on each frame to precisely locate the target on the detector, which will be useful in a second stage for mitigating the photometric systematics. We finally perform simple aperture photometry on individual frames, with star and sky apertures centered on the target position determined in the previous step. We test different aperture sizes and use a portion of the light curve to measure the rms and level of correlated noise (e.g., Demory et al. 2016) to determine the aperture that minimizes both quantities. We eliminate outliers based on data points having significant positive median absolute differences (Hoaglin et al. 1983) from the median. The remainder of the data is then ingested into a Markov Chain Monte Carlo (MCMC) framework that includes a polynomial detrending from the centroid position (Demory et al. 2011) previously measured, as well as longer-term trends that are of instrumental or astrophysical origin. The MCMC fit computes uncertainties that include the contribution from correlated noise in the data (Winn et al. 2008; Gillon et al. 2010) and errors in coefficients used in the polynomial detrending. The photometric rms is then computed on the final, detrended light curve. We perform further attempts to improve the light curve extraction by using custom, non-circular-shaped apertures for some targets. A non-circular aperture avoids inclusion of pixels that contains mostly background noise. For this step, we compute for each target a baseline flux value that corresponds to the median of the pixel fluxes where no star is detected, thus containing only background signal. We then define the photometric aperture by selecting only the pixels located at the target location with flux values larger than the median background flux multiplied by a coefficient that is based on the target’s magnitude. We find this approach results in a slightly better photometric rms for the fainter objects of our sample. We finally compare our photometric reduction with publicly available corrected light curves (*K2SC*, *K2SFF*, *K2VARCAT*; Vanderburg & Johnson 2014; Aigrain et al. 2016; Armstrong et al. 2016), all available from MAST. We randomly select 10 targets across our sample and find the photometric rms to be consistent between these three methods and ours.

3.2. Planet Search

We then perform a transit search using a box least-squares fitting algorithm (BLS; Kovács et al. 2002). We set the BLS to orbital periods ranging from 0.8 days to half of the duration of the campaign (~40 days). The ratio of the transit duration over the planet orbital period is further set between 0.0007 and 0.06 to include a wider range of orbital periods, eccentricities, and impact parameters than the T-1bc planets. We note that the transit duration of planets orbiting LMDs can be as short as 20 minutes for 1 day orbital periods. Because of the *Kepler* 30 minute cadence photometry, these transits appear significantly smeared out. Long-cadence data could thus potentially hamper the detectability of close-in planets with short transit durations. Our pipeline returns for each star the raw/corrected photometry, the stellar motion over the entire campaign duration, and the transit search results.

Among the 189 LMDs that are part of our sample, our BLS analysis yields no transiting candidate detection at a 4σ detection level or above. We explore the possible reasons for this null result below.

4. TRANSIT INJECTION TESTS

In the following we explore whether the null result regarding our transit search is due to an insufficient sensitivity of *K2* to planets transiting LMDs. More specifically, in the light of the recent discovery of T-1, we investigate whether our data set is able to put constraints on the frequency of tight planetary systems orbiting LMDs.

4.1. Recovery of TRAPPIST-1-like Systems

We first model a light curve of T-1b ($P = 1.51$ days, $R_p = 1.11 R_{\oplus}$) and c ($P = 2.42$ days, $R_p = 1.05 R_{\oplus}$) using the system parameters published in Gillon et al. (2016). While the transits are modeled using a 30 s cadence, we integrate them to the *K2* 30 minute long-cadence at which the observations are obtained. The T-1bc planets are then injected in the *K2* raw photometry, just after the flux extraction from the TPF files. The transit depths are multiplied by a factor that is the squared ratio of stellar radius between T-1 and the target. We then perform the different steps detailed in Section 3.1 with the exact same sequence. The goal of this part of the analysis is to assess how frequently we detect T-1b and c planets, together or separately. We run the BLS analysis a first time, identify the signal with the maximum signal-to-noise ratio in the periodogram, remove the corresponding data from the corrected phased-light curves and run a second BLS analysis. We consider each planet to be successfully recovered if the deduced orbital period matches the input model transit data at 2% or less.

Across the 189 systems that are part of our sample, we find that we are able to recover T-1b and T-1c for 20 (11%) and 12 (6%) targets respectively. For most cases, the Poisson noise is too large to enable a clear detection of the planets injected in the photometry, leading to false alarms. We find as well that, as expected, the depth recovered by the BLS is impacted by the data sampling. For both T-1b and c, a single photometric point only is located in transit, and since the orbital period of the planet is not an exact multiple of 30 minutes, the in-transit point shifts in phase, hence its apparent depth. This reduces the peak power in the BLS spectrum and artificially reduces the strength of the planetary signal.

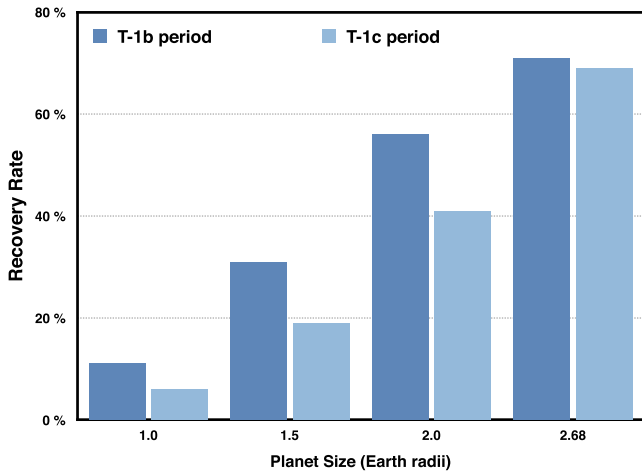


Figure 2. Recovery rates for TRAPPIST-1 planets. This histogram shows the percentage of recovery for planets that have been injected in the LMDs that are part of our sample. The dark and light bars are the recovery rates for planets with the orbital periods of T-1b and T-1c, respectively, assuming radii spanning 1–2.68 R_{\oplus} .

4.2. Sensitivity to “Inflated” TRAPPIST-1-like Systems

We repeat the same analysis as above but injecting this time planets with radii that are $1.5\times$ and $2\times$ larger than the T-1bc planets, while retaining all other orbital properties. We find that for a 1.5 scale factor, the recovery rate is 31% for T-1b and 19% for T-1c. Injecting transits of planets that are twice as large yields recovery rates of 56% and 40% for T-1b and T-1c, respectively.

We finally conduct injection tests of planets similar to GJ 1214b in size, using a published radius of $2.68 R_{\oplus}$ (Charbonneau et al. 2009) for both T-1b and T-1c. We find in that case recovery rates of 71% and 67% for T-1b and T-1c, respectively.

All recovery rates are shown in Figure 2 for T-1b and T-1c. We show in Figure 3 the Kp magnitude distribution of target stars (gray) and superimpose the subsample for which the signal is recovered (black) for a planet with a size equal to T-1b (left) and GJ 1214b (right).

5. PLANET FORMATION MODELS

We have computed planet formation models in the framework of the core-accretion scenario, focusing on LMDs ($0.1 M_{\odot}$). Our model is based on the models of Alibert et al. (2013) and Fortier et al. (2013). They both take into account the structure of the protoplanetary disk and its evolution, the migration of the planet, as well as the computation of the planetary growth and composition.

The mass of the star is included in the models via different aspects (Alibert et al. 2011), the most important being the distribution of the disk masses, which is different from the one used for solar-type stars, and follows the relation

$$M_{\text{disk}} \propto M_{\text{star}}^{1.2}. \quad (1)$$

Figure 4 shows the radius distribution resulting from our models, for planets inside 0.1 au. As can be seen in Figure 4, the distribution of radii extends from ~ 0.5 to $\sim 1.4 R_{\oplus}$, with the majority of planets having a radius of the order of $1 R_{\oplus}$ or smaller. These values are similar to the ones of the recently discovered T-1bcd planets (Gillon et al. 2016), and we find no

planet to be formed with a substantially larger radius. As shown in Figure 4, the recovery rate for these synthetic planets is expected to be small (of the order of 20% maximum).

Some of these planets harbor a non-negligible fraction of water because they start their formation process beyond the iceline (the iceline is located between ~ 0.2 and ~ 1 au, depending on the mass of the protoplanetary disk). Interestingly, precise enough determination of the planetary bulk density can allow the determination of the fraction of volatiles, for the shortest-period planets. Indeed, if evaporation is efficient enough, short-period low-mass planets cannot retain a gas atmosphere, and the degeneracy in the determination of the planetary composition is reduced (Alibert 2016).

6. DISCUSSION

6.1. K2 Sensitivity to TRAPPIST-1-like Systems

The first conclusion of this Letter is that across the 189 LMDs that are part of our sample, we would have been able to detect the T-1 b and c planets for only $\sim 10\%$ of the targets. Our pipeline efficiently takes correlated noise and stellar variability into account. The dominant source of noise is mostly white and points to the limited performance of K2 to obtain precision photometry for cool and faint LMDs.

Assuming that each star was hosting such a system (occurrence rate of 1), and assuming a 100% recovery rate and a geometric transit probability of $\sim 5\%$ for these systems, we should have detected about 5 systems per 100 targets. However, the fact that our recovery efficiency on this sample for T-1-like systems is only 10% means that we would have recovered 0.95 systems across our sample, which is consistent with our non-detection. We estimate that a total of ~ 1000 well-characterized LMDs will be observed by the end of 2018 by K2. If the trend in occurrence rate of planets orbiting *Kepler* early M stars (Dressing & Charbonneau 2013) extends into the LMD regime, we should expect K2 to be able to detect up to ~ 5 of these Earth-size systems within the next 2 years. However, if the occurrence rate of TRAPPIST-1-like systems is lower than 20%, no detections from K2 are expected.

Figure 3 (left) shows that K2 sensitivity to T-1b-like planets orbiting LMDs extends to $K_p \sim 20$, and the recovery rate decreases in a Poisson-limited regime down to the tail of the sample magnitude distribution (i.e., Poisson-limited performance yields no detections for $K_p > 20$).

6.2. A Possible Lack of Close-in Super-Earth-size Exoplanets Orbiting Late M Dwarfs

The second conclusion of this Letter is that despite our ability to detect companions larger than the T-1bc planets orbiting the LMDs, we find no objects that are 1.5 times the size of the T-1b or larger. When injecting T-1bc planets with 1.5 times the size of the Earth (super-Earth regime), we find that these planets are fully recovered for $\sim 31\%$ of the target sample for orbital periods similar to T-1b. We should thus have found $31\% \text{ recovered} \times 189 \text{ hosts} \times 5.4\% \text{ transit probability} = 3.2$ planets, assuming an occurrence rate of 1. Similarly, when using a size factor of 2.0 rather than 1.5, we would have found 5.7 such “inflated” T-1b-like planets within our sample.

The cause for this null result regarding the planet search in the present sample could be multi-fold. First, larger exoplanets may orbit farther from their host, thus reducing their probability

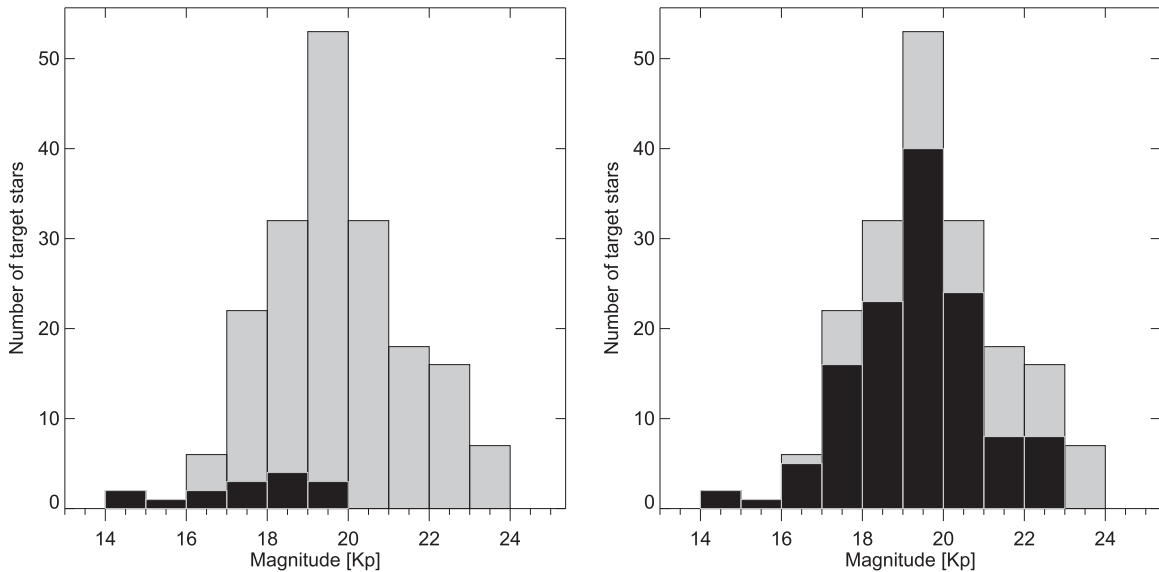


Figure 3. Detectability of TRAPPIST-1b-like planets. Distribution of targets included in our sample (gray). Left: distribution of targets for which the injected T-1b signal is correctly recovered (black). Right: distribution of targets for which the injected planet with a period equal to T-1b but with $R_p = 2.68R_{\oplus}$ is correctly recovered (black).

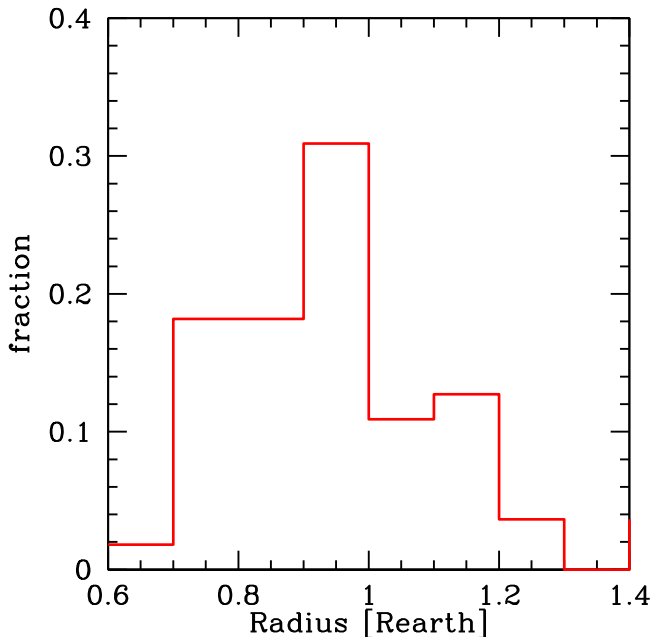


Figure 4. Planetary radii for planets orbiting a T-1-like star from the formation models of Alibert et al. (2013) and Fortier et al. (2013). Distribution of planet radii, for planets located inside 0.1 au of the central star. The radius is computed using the method presented in Alibert (2014).

of transit significantly, which would render our observations consistent with non-detections. Second, the distribution of the frequency of planets around LMDs may peak toward smaller radii than it does for more massive hosts, as suggested from planet formation models (Section 5). Assuming that the ratio of the disk mass to the host star mass is constant from solar to the brown-dwarf regime, as shown from FIR observations of young systems (e.g., Mohanty et al. 2013), LMDs would form mostly small planets. Third, the occurrence rate for these planets may be significantly smaller than 1.

It is worth noting as well that for a given data set we have 1.6 times the number of transits of T-1b compared to T-1c and both have similar depths. Thus, we would expect, all other things being equal, to have a ratio in recovery rates of 1.3. We find that this factor does not fully explain the discrepancy in recovery rate for our injection tests of Earth-size planets but accounts for the difference in recovery ratio between T-1b and T-1c for the 1.5 and 2.0 Earth radii particularly well (see Section 4). This suggests that the light curves are dominated by Poisson statistical noise, except for the lower amplitude signals, where residual correlated noise of astrophysical or instrumental origin likely complicate the retrieval of the individual transits. Another useful check is to compute the ratio of recovered signals versus the planetary sizes. For 1.5 and 2.0 size factors, the corresponding transit depth is 2.25 and 4 times larger. From our T-1b recovery rates of 11%, 31%, and 56%, the corresponding factors are 2.8 and 5.1, which are both in good agreement. For T-1c, the recovery rates are 6%, 19%, and 40%, yielding factors of 2.7 and 5.8, suggesting that the shorter period of T-1b makes its recovery easier especially for small planetary sizes.

6.3. A Lack of Close-in Mini-Neptune Exoplanets Orbiting Late M Dwarfs

The third conclusion of this paper is that while *K2* has excellent sensitivity to mini-Neptune exoplanets, similar in size to GJ 1214b, none are found in our sample. Our injection tests confirm, however, that these objects would have been found in our sample and we would have expected to find $71\% \text{ recovered} \times 189 \text{ hosts} \times 5.4\% \text{ transit probability} = 7.2$ planets, assuming an occurrence rate of 1 planet per star. Our findings suggest that the occurrence rate of mini-Neptunes orbiting LMDs is likely an order of magnitude smaller at least, making them rare around this population of targets, similar to early-/mid- and late-M stars as shown by observations (Berta et al. 2013; Dressing & Charbonneau 2013) and models (Section 5), respectively. Contrary to T-1b-like planets, Figure 3 (right) shows that the detectability of GJ 1214b-like planets orbiting

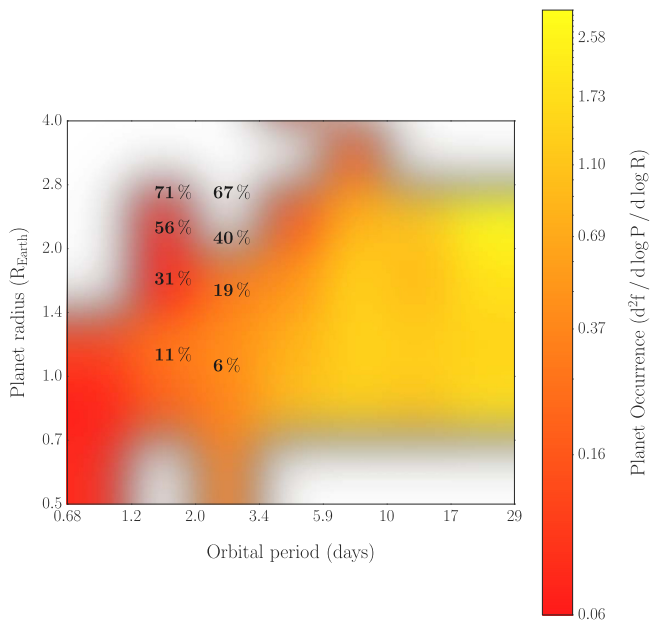


Figure 5. Planet occurrence and *K2* recovery rate. The planet occurrence rate from Dressing & Charbonneau (2013) is shown in colored scale (low to high, red to yellow). White areas represent the absence of detections in the corresponding period-radius bins. The recovery rate (in percent) of planets injected in our sample LMDs at the orbital periods of T-1b and c are shown superimposed for different planet radii.

LMDs extend to $K_p \sim 23$ and that the limitation is not from Poisson noise anymore. Rather, the recovery rate is almost constant between $K_p \sim 16$ and 21 and drops afterward. We find that no GJ 1214b-like planet is recovered beyond $K_p \sim 23$, which is consistent with our sensitivity for T-1b-like planets discussed at the beginning of this section. The origin of this plateau is thus due to a non-optimal recovery rate at the mid-magnitude range of our sample before Poisson-limited noise dominates again, possibly due to a larger activity level of a subsample of our targets.

We show a summary of our findings in Figure 5. This diagram shows the occurrence rate of *Kepler* planets published for early- and mid-M stars (Dressing & Charbonneau 2013) and the superimposed numbers indicate our recovery rate (in percent) at the orbital periods of T-1b and c for different planet radii. Assuming that this occurrence rate distribution extends into the LMD regime, Figure 5 shows that *K2* is relatively inefficient at detecting planets with radii $R_p \lesssim 1.4R_{\oplus}$, where the occurrence rate peaks for 1.51 (T-1b) and 2.42 (T-1c) days. However, formation models produce only few planets at separations smaller than <0.05 au (Figure 4). If models are right, it means that there is a strong transition in the occurrence rate of planets between early- and late-type M dwarfs and that the discovery of T-1 out of ~ 50 targets monitored in the TRAPPIST survey had a very low probability of detection. Alternatively, models could be missing important ingredients that future monitoring of similar systems may help to constrain.

K2 relies on its ability to quasi-continuously monitor several thousands of targets over 80 days for each campaign. By the

end of 2018, we may expect *K2* to discover one or two systems similar to T-1 and a handful of super-Earth systems if their occurrence rate is similar to the one deduced from the *Kepler* primary mission’s M stars. We finally note that we have proposed *K2* observations of TRAPPIST-1 in Campaign 12. Because this target is bright, it is part of the 10% subsample for which we will be able to precisely characterize the transits of the known planets and search for other companions in this remarkable system.

Part of this work has been carried out within the frame of the National Centre for Competence in Research PlanetS supported by the Swiss National Science Foundation. Y.A. acknowledges the financial support of the SNSF. M.G. is Research Associate at the Belgian F.R.S-FNRS. We thank the anonymous referee for a helpful review. This paper includes data collected by the *K2* mission. Funding for the *K2* mission is provided by the NASA Science Mission directorate.

Facility: Kepler.

REFERENCES

- Aigrain, S., Parviainen, H., & Pope, B. J. S. 2016, *MNRAS*, 459, 2408
 Alibert, Y. 2014, *A&A*, 561, A41
 Alibert, Y. 2016, *A&A*, 591, A79
 Alibert, Y., Carron, F., Fortier, A., et al. 2013, *A&A*, 558, A109
 Alibert, Y., Mordasini, C., & Benz, W. 2011, *A&A*, 526, A63
 Armstrong, D. J., Kirk, J., Lam, K. W. F., et al. 2016, *MNRAS*, 456, 2260
 Baraffe, I., Homeier, D., Allard, F., & Chabrier, G. 2015, *A&A*, 577, A42
 Berta, Z. K., Irwin, J., & Charbonneau, D. 2013, *ApJ*, 775, 91
 Charbonneau, D., Berta, Z. K., Irwin, J., et al. 2009, *Natur*, 462, 891
 Cruz, K. L., & Reid, I. N. 2002, *AJ*, 123, 2828
 Cruz, K. L., Reid, I. N., Kirkpatrick, J. D., et al. 2007, *AJ*, 133, 439
 Cruz, K. L., Reid, I. N., Liebert, J., Kirkpatrick, J. D., & Lowrance, P. J. 2003, *AJ*, 126, 2421
 Demory, B.-O., Gillon, M., Deming, D., et al. 2011, *A&A*, 533, 114
 Demory, B.-O., Gillon, M., Madhusudhan, N., & Queloz, D. 2016, *MNRAS*, 455, 2018
 Demory, B.-O., Seager, S., Lissauer, J., et al. 2013, arXiv:1309.1078
 Dressing, C. D., & Charbonneau, D. 2013, *ApJ*, 767, 95
 Fortier, A., Alibert, Y., Carron, F., Benz, W., & Dittkrist, K.-M. 2013, *A&A*, 549, A44
 Gillon, M., Jehin, E., Lederer, S. M., et al. 2016, *Natur*, 533, 221
 Gillon, M., Lanotte, A. A., Barman, T., et al. 2010, *A&A*, 511, 3
 Hoaglin, D., Mosteller, F., & Tukey, J. 1983, *Understanding Robust and Exploratory Data Analysis* (New York: Wiley)
 Howell, S. B., Sobek, C., Haas, M., et al. 2014, *PASP*, 126, 398
 Koch, D. G., Borucki, W. J., Basri, G., et al. 2010, *ApJL*, 713, L79
 Kovács, G., Zucker, S., & Mazeh, T. 2002, *A&A*, 391, 369
 Lodieu, N., Hambly, N. C., Jameson, R. F., et al. 2007, *MNRAS*, 374, 372
 Mohanty, S., Greaves, J., Mortlock, D., et al. 2013, *ApJ*, 773, 168
 Payne, M. J., & Lodato, G. 2007, *MNRAS*, 381, 1597
 Reid, I. N., Cruz, K. L., & Allen, P. R. 2007, *AJ*, 133, 2825
 Reid, I. N., Cruz, K. L., Kirkpatrick, J. D., et al. 2008, *AJ*, 136, 1290
 Reiners, A., & Basri, G. 2010, *ApJ*, 710, 924
 Seager, S. 2014, *PNAS*, 111, 12634
 Slesnick, C. L., Carpenter, J. M., & Hillenbrand, L. A. 2006, *AJ*, 131, 3016
 Slesnick, C. L., Hillenbrand, L. A., & Carpenter, J. M. 2008, *ApJ*, 688, 377
 Vanderburg, A., & Johnson, J. A. 2014, *PASP*, 126, 948
 West, A. A., Hawley, S. L., Bochanski, J. J., et al. 2008, *AJ*, 135, 785
 West, A. A., Weisenburger, K. L., Irwin, J., et al. 2015, *ApJ*, 812, 3
 Winn, J. N., Holman, M. J., Torres, G., et al. 2008, *ApJ*, 683, 1076